
Article:
Ryabenkova, Y, Jadav, N, Conte, M. et al. (5 more authors) (2017) Mechanism of Hydrogen-Bonded Complex Formation between Ibuprofen and Nanocrystalline Hydroxyapatite. Langmuir. ISSN 0743-7463

https://doi.org/10.1021/acs.langmuir.6b04510

The mechanism of hydrogen-bonded complex formation between ibuprofen and nanocrystalline hydroxyapatite.

*Yulia Ryabenkova[a], Niten Jadav[b], Marco Conte[c], Michael Hippler[c], Nik Reeves-McLaren[d], Phil Coates[a], Peter Twigg[a], Anant Paradkar[b]**

[a]School of Engineering, University of Bradford, Bradford, BD7 1DP, UK

[b]Centre for Pharmaceutical Engineering Science, University of Bradford, Bradford, BD7 1DP, UK

[c]Department of Chemistry, University of Sheffield, Sheffield, S3 7HF, UK

[d]Department of Materials Science and Engineering, University of Sheffield, Sheffield, S1 3JD, UK.

KEYWORDS

Hydrogen bonding, mechanistic studies, ibuprofen, hydroxyapatite, drug delivery, dissolution

ABSTRACT

Nanocrystalline hydroxyapatite (nanoHA) is the main hard component of bone and has potential to be used to promote osseointegration of implants and to treat bone defects. Here, using active pharmaceutical ingredients (APIs) like ibuprofen, we report on the prospects of combining nanoHA with biologically active compounds to improve the clinical performance of these treatments. In this study we designed and investigated the possibility of API attachment to the surface of nano-HA crystals via the formation of a hydrogen-bonded complex. The mechanistic studies of an ibuprofen/nanoHA complex formation have been performed using a holistic approach encompassing spectroscopic (FT-IR and Raman) and X-ray diffraction techniques as well as quantum chemistry calculations (DFT), while comparing the behaviour of the ibuprofen/nanoHA complex with that of a physical mixture of the two components. Whereas ibuprofen exists in dimeric form both in solid and liquid state, our study showed that the formation of the ibuprofen/nanoHA complex most likely occurs via the dissociation of the ibuprofen dimer into monomeric species promoted by ethanol, with subsequent attachment of a monomer to the HA surface. An adsorption mode for this process is proposed; this includes hydrogen bonding of the hydroxyl group of ibuprofen to the hydroxyl group of the apatite, together with the interaction of the ibuprofen carbonyl group to an HA calcium centre. Overall, this mechanistic study provides new insights into the molecular interactions between APIs and the surfaces of bioactive inorganic solids and sheds light on the relation between the non-covalent bonding and drug release properties.

1 Introduction

Hydroxyapatite, with its chemical formula $Ca_{10}(PO_4)_6(OH)_2$, is a major inorganic component of the bone and, along with collagen fibrils, it accounts for up to 65% of the hard tissue of vertebrates. Bone-derived hydroxyapatite is nanosized, non-stoichiometric, calcium-deficient carbonated ceramic material with low crystallinity [1]. Synthetic poorly crystalline nanoscale hydroxyapatite that mimics the composition of natural bone has long been employed in orthopaedics for the treatment of bone defects resulting from trauma or surgery as it possesses excellent biocompatibility and osteoconductivity properties [2], thus showing a great potential for the use in bone tissue engineering [3], implant osseointegration [4] as well as being a potential gene [5] or drug carrier [6, 7].

Drug delivery systems based on ceramics [8, 9], polymers [10] or hydrogels [11] have received an enhanced interest in the last decades. Hydroxyapatite based ceramic drug carriers, in turn, have been particularly studied as prospective drug delivery systems for the treatment of bone infection [12, 13] as well as arthritis [14]. Osteoarthritis and rheumatoid arthritis, despite having different causes behind the diseases, share similar symptoms of chronic pain due to associated peripheral inflammation. Both are considered an important public health concern [15], with osteoarthritis being the most common cause for total hip or knee replacement. The results of total arthroplasty in arthritic patients shows that HA coated prostheses have excellent medium-term efficacy [16], promoting osseointegration and in turn opening up the prospects of using bioactive ceramics as drug carriers for the treatment of bone diseases.

One of the most common analgesic anti-inflammatory non-steroidal drugs used for relief of pain symptoms in arthritic patients is ibuprofen [17]. Ibuprofen, or 2-(4-isobutylphenyl) propanoic acid (Fig. 1a), exists as a cyclic hydrogen-bonded dimer in a solid state (Fig. 1b) [18]

and its anti-inflammatory and analgesic activity is assigned to the mono-carboxyl groups of an ibuprofen monomer [19]. Based on this, it is beneficial to introduce ibuprofen into the body as a monomer, for instance as a sodium salt [20], for an improved performance due to a higher drug solubility.

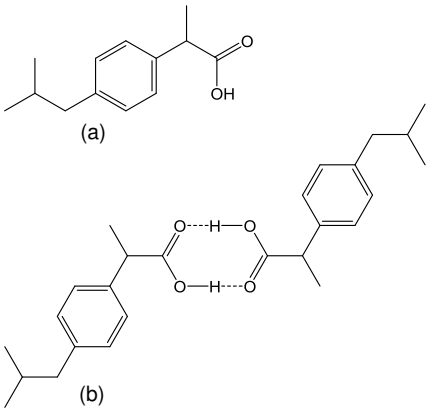

Figure 1. Structures of: (a) ibuprofen monomer, 2-(4-isobutylphenyl) propanoic acid, and (b) dimer of ibuprofen highlighting the hydrogen bond between carboxyl groups.

Several attempts have been made to combine hydroxyapatite and ibuprofen for treating bone-associated diseases, possibly in a monomeric state to achieve the desired drug dissolution rates [21, 22]. These studies attempt to relate the prolonged retention times and drug release either with the geometry of the materials [23] or with the porosity of ceramics [24] in combination with hydrogen bonding effects between hydroxyapatite and ibuprofen monomer. Whereas the majority of studies produced materials using a trial-and-error approach to find the best possible combination of an API and an excipient, they did not focus on the mechanism of the API adsorption and release, but rather on the final formulation with certain characteristics. However, to the best of our knowledge there are currently no insights into the physical chemistry behind the ibuprofen loading onto the surface of hydroxyapatite and its release. In this paper we report for the first time on mechanistic studies describing the adsorption of ibuprofen on the surface of

hydroxyapatite and propose a possible mechanism for the interaction of ibuprofen and hydroxyapatite at the molecular level. The understanding of the surface properties of ceramics and its influence on the API dissolution rates may provide a useful conceptual platform for the rational development and design of formulations with the desired controlled and sustained drug release.

2 Materials and methods

2.1 Nano-hydroxyapatite preparation.

Nano-hydroxyapatite was prepared as reported in [25] and references therein. In brief, calcium hydroxide $Ca(OH)_2$ (3.704 g, assay ≥96%, Sigma Aldrich) and phosphoric acid H_3PO_4 (3.459 g, 85% wt. in water, Sigma Aldrich) were dissolved in 100 ml of deionised water each. The solution of phosphoric acid was fed into the solution of calcium hydroxide at room temperature using a peristaltic pump at a rate of 3 $ml \cdot min^{-1}$. The resulting slurry was left under constant stirring for 2 hours for ageing and left overnight for settling. The top aqueous layer was then removed and the suspension was dried at 60 °C and subsequently ground using an agate mortar and pestle to form a powder. A portion of the powder was calcined for 2 h in a furnace at 1000 °C (with a heating rate of 10 $°C \cdot min^{-1}$) in order to evaluate its thermal stability.

2.2 Ibuprofen/nano-hydroxyapatite complex synthesis.

To prepare an ibuprofen/HA complex the following procedure was employed. Ibuprofen (200 mg, grade 70 UPS/EP, Albemarle) was dissolved in anhydrous ethanol (5 ml, absolute 99%+, Fisher) in a 19/26 joint 100 ml round bottom flask. A sample of dried as-prepared nanoHA (800 mg) was added to the solution and stirred in a Buchi Rotavapor at 30 °C and 350 mbar for 1 hour at a speed of 60 rpm. Then the temperature was raised to 45 °C and the pressure reduced to 175

mbar to reach the condition of a very viscous paste (to avoid complete evaporation of ethanol). The reproducibility of the method was evaluated using ATR-FTIR experiments for each sample to confirm the presence of monomeric, dimeric and attached species (where applicable). The reason behind opting for the 20wt% loading is explained in the supplementary data file (Fig. S1). An aliquot of the paste was used for *in situ* and *ex situ* spectroscopic studies, whereas the remaining part was dried at room temperature for 24 hours and used for morphological examination.

2.3 Materials characterisation.

Fourier Transform Infrared (FTIR) spectra were acquired using a ThermoFisher Nicolet iS50 FTIR spectrophotometer equipped with a single reflection diamond attenuated total reflection (ATR) module. Spectra were recorded in the absorbance mode from 4000 to 375 cm^{-1} at 1 cm^{-1} resolution averaging 64 scans.

X-ray powder diffraction (XRPD) patterns were acquired using a Bruker D8 Advance Diffractometer operating at 40 kV and 40 mA with Cu K_α radiation. In order to minimise preferred orientation of crystallites within specimens, XRPD data were collected in Debye-Scherrer mode for ibuprofen-containing samples mounted in silica glass capillaries using a PANalytical X'Pert^3 Powder diffractometer with Cu K_α radiation operating at 45kV, 40mA, and a Medipix^3 Pixcel1D detector. The samples were analysed in the range of either 20 to 60° 2θ for nanoHA characterisation or from 0 to 80° 2θ for ibuprofen and ibuprofen/HA complexes. Analysis of the obtained patterns was carried out using X'Pert HighScore Plus software, and stripping of the $K_{\alpha 2}$ component was carried out when appropriate. Crystallite sizes for the hydroxyapatite were determined using the Scherrer equation [26], and XRPD patterns were

compared with entries of the International Centre for Diffraction Data (ICDD) Powder Diffraction File (PDF).

Raman spectra were obtained using a home-built Raman spectrometer as described in [27], but with the following modifications: using a frequency doubled Nd:YAG laser, 532.2 nm, 20 mW (Lasos, GL3dT) and a monochromator (Andor SR-163) equipped with 1200 l/mm grating, 500 nm blaze, and cooled CCD camera (Andor i-Dus, - 60 °C).). Effective slit width is given by a 100 μm core diameter fibre. Wavenumber calibration was performed using Ne emission lines and known benzene Raman transitions (NIST database, [28]). Experimental resolution was approximately 8 cm^{-1} full width at half maximum (FWHM) around 1700 cm^{-1} Raman shifts; Raman peak position accuracy was estimated to be ± 3 cm^{-1}.

Scanning electron microscopy (SEM) images were recorded using a Hitachi TM3000 electron microscope operating at 15 kV. All samples were sputtered with gold prior to analysis.

Dissolution experiments were performed using a UPS II type Labindia dissolution tester (Labin-09, India). Ibuprofen/HA complex, physical mixture of ibuprofen and HA or raw ibuprofen powders were placed at the bottom of the dissolution vessel (at least four repeats) containing 900 ml phosphate buffer (pH 7.2) maintained at 37 ± 0.5 °C and stirred with a paddle at 50 rpm. Samples were collected periodically and further filtered. Quantification of ibuprofen was performed spectrophotometrically at a fixed wavelength of 221 nm using a Jasco-V630 spectrophotometer.

^{1}H-NMR experiments were recorded at 400 MHz using a Bruker Avance III 400 spectrometer. Measurements were collected at room temperature for solutions of ibuprofen in $CDCl_3$ or CD_3CD_2OD (Sigma Aldrich). Fitting of the NMR peaks was carried out using Bruker TopSpin

3.2 software, and data analysis was carried out by using a successive approximation method based on fixed-point iteration algorithm.

2.4 Computational studies.

Quantum chemical calculations were performed using Gaussian 09, version D.01 [29]. Density functional theory (DFT) [30] method using the B3LYP functional and a 6-311G(d,p) basis set (Pople triple split valence Gaussian basis functions with added polarization functions) for all atoms have been employed [31]. The nature of stationary states (minimum structures) was confirmed by frequency calculations. Stabilization energies of the complexes were obtained by subtraction from energetic values of isolated species and considering zero point energy (ZPE) corrections [32] for all of the molecular structures. Calculated wavenumbers to compare with experimental infrared spectra were obtained from harmonic vibrational frequencies using the B3LYP density functional method with the 6-311G(d,p) basis set by introducing a scaling factor of 0.9616 [33].

3 Results and discussion

3.1 NanoHA characterisation.

The inorganic part of bone is mainly made of a nano-dimensional non-stoichiometric poorly crystalline hydroxyapatite phase with small inclusions of carbonate [1]. Several characterisation techniques were employed to verify whether the synthesised ceramics mimic the bone composition. Fig.S2 shows the XRD pattern of both as-prepared and calcined hydroxyapatite. It can be seen that the raw material (Fig. S2a) is made solely of hydroxyapatite phase that fully matches JCPDS entry 9-432 (for a visualization of its unit cell see Fig. S3). The broad reflection peaks on the XRD patterns in the region between 20 and 50° 2θ are usually characteristic of

either partially amorphous or nano-particulate material. Interestingly, Fig. S2b reveals that the composition of the materials has changed after calcination. Besides the main phase of hydroxyapatite, another phase of tri-calcium phosphate, or TCP (JCPDS entry 9-169), appeared. This is caused by the decomposition of the non-stoichiometric hydroxyapatite into β-calcium phosphate [34]. Crystallinity calculations, in turn, showed that the raw, or as-prepared HA, is made of *ca.* 35% crystalline component, whereas the crystallinity of the calcined HA expectedly reached *ca.* 96% after a prolonged heat treatment (Table 1).

Material	Unit cell parameters (Å)			Unit cell, V(Å^3)	Crystallite size (nm)	Crystallinity (%)	HA phase purity (wt %)
	a	*b*	*c*				
HA raw	9.439	9.439	6.887	531.4 ± 1.1	13	35	100
HA calcined	9.403	9.403	6.876	526.5 ± 1.1	79	96	77(*)

Table 1. Unit cell parameters from Rietveld refinement and crystallinity evaluations of nano-hydroxyapatite as-synthesised and calcined at 1000 °C. Contraction of the unit cell upon calcination is observed as well as increase in crystallinity. A second phase, namely tri-calcium phosphate or TCP, has also been detected after thermal treatment, showing non-stoichiometry of the as-prepared HA. (*)23 wt% attributed to the tri-calcium phosphate (JCPDS entry 9-169).

According to the Rietveld refinement results for the lattice parameters, the calculated unit cell of the raw hydroxyapatite was 531.4 ± 1.1 Å^3 whereas for the calcined material it was 526.5 ± 1.1 Å^3, while the proportion of the second phase of tri-calcium phosphate (TCP) was 23 wt. %. The Scherrer equation [26], allowed us to evaluate the crystallite size which appeared to be 13 nm for raw HA and 79 nm for calcined HA. Decomposition of HA into TCP after thermal

treatment and reduction of the unit cell volume is indirect evidence of its non-stoichiometry, whereas its particle (crystallite) size lies within a nanometer range, thus proving that the HA used for this study is indeed a non-stoichiometric nano-sized material with poor crystallinity.

To further prove its similarity to the HA in the bone we used an attenuated total reflectance (ATR) FTIR technique as XRD alone, being a bulk method, cannot reveal all the details of the HA composition, especially for the layers of solid close to its surface. ATR-FTIR is a spectroscopic technique where an IR beam is directed at a solid sample and is further reflected to a detector [35]. An important aspect of this method is that this technique is often regarded as a 'surface' method with a penetration depth in the range of 0.5 to 3 μm [36]. That is, the method is a surface technique when compared to XRD, but not a pure surface analysis method like X-ray photoelectron spectroscopy which probes 0.5-10 nm instead. However, considering that our HA is present in the form of agglomerates ranging from 20 to 200 μm and that ibuprofen is also in a similar range (vide infra, Fig. 3), we can ascribe the use of ATR-FTIR as a surface method, but with a large penetration depth. This particular aspect of the technique will be important also for the investigation of the mechanism of adsorption of ibuprofen to the HA surface (see section 3.4.4).

An ATR-FTIR spectrum of raw hydroxyapatite is reported in Fig. S4. The main active bands lie in the region of 1100-400 cm^{-1}, with the typical phosphate stretching bands lying in the range 1200-900 cm^{-1}, as well as around 600 cm^{-1}, being in agreement with previously published data, hydroxyl group vibrations are located at 3571 and 632 cm^{-1} [37-39]. Minor carbonate substitution of B-type (CO_3^{2-} for PO_4^{3-}) was also detected with the corresponding peaks for bending and stretching modes at 870 cm^{-1} and 1600-1300 cm^{-1} respectively, thus suggesting that the surface carbonate formation occurred during the preparation despite the fact that carbonate

anions were not deliberately introduced into the system. This is a known phenomenon where CO_2 capture from the atmosphere may occur when one of the solutions has high pH values [40] or a strongly basic surface in the presence of moisture. Overall, the presence of small amounts of carbonate groups on the surface of HA is characteristic for the wet precipitation preparation method. However, our results are slightly different from previously reported studies where it has been suggested that A-type carbonate substitution (CO_3^{2-} for OH^-) occurs at lower temperatures, whereas B-type substitution is a feature of the materials prepared at elevated temperature ranges [25]. We observed only a slightly detectable A-type substitution with the B-type dominating, thus suggesting that the material mostly mimics the young bone tissue [41] as the ratio of A/B types is age dependent and also influences the HA crystallinity and solubility [42].

3.2 Ibuprofen/HA complex formation.

In order to prepare an ibuprofen-hydroxyapatite complex we opted for dissolution of the API in ethanol with subsequent solvent evaporation under vacuum and deposition of ibuprofen onto the ceramic's surface while drying in a Rotavapor [43]. The reason behind such a choice is twofold. Firstly, ethanol is a much more "green" solvent with minimal environmental impact in chemical production compared to the widely used hexane, yet it still allows successful solubilisation of ibuprofen. Secondly, the solvent evaporation process allows us to control the API loading and eliminates the need of post-process API content measurement (as in the case of immersion of HA into hexane with dissolved ibuprofen [21]), as there is no API loss during the preparation and the ibuprofen uptake is independent of the porosity properties of the ceramic.

With the aim of evaluating the possibility of API attachment to the surface of hydroxyapatite we employed a wide variety of methods. Firstly, we wanted to assess the homogeneity of the ibuprofen distribution on the surface of ceramics. Fig. 2 shows the comparison of XRD patterns

between as-prepared HA (a), pure ibuprofen from the supplier (b), ibuprofen recrystallized from ethanol using the method of ibuprofen/HA complex preparation with the ceramic addition step being omitted (c), and ibuprofen-hydroxyapatite complex itself (d).

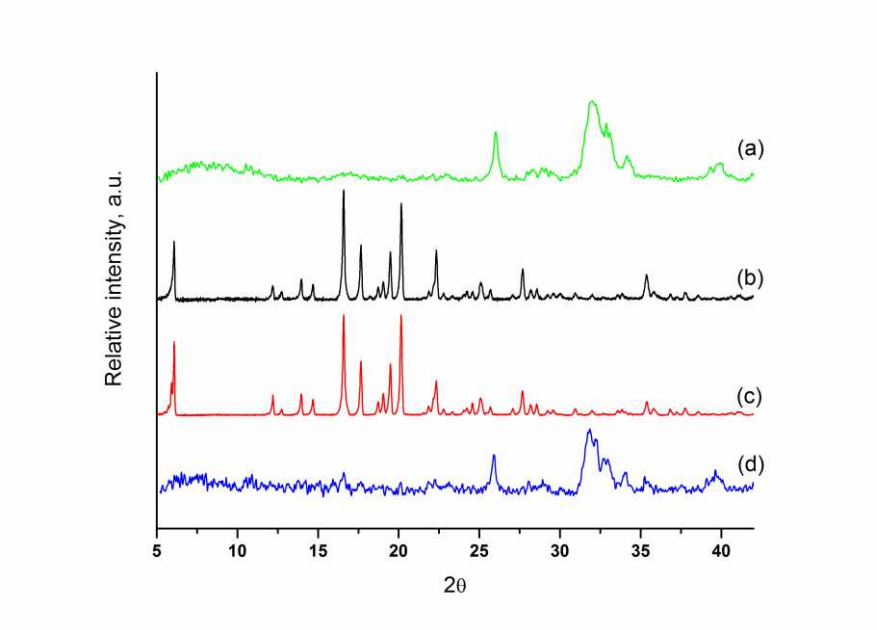

Figure 2. XRPD patterns of: a) raw hydroxyapatite, b) commercial, or as received, ibuprofen from the supplier, c) commercial ibuprofen recrystallized in ethanol, d) ibuprofen/hydroxyapatite (ibuprofen/HA) complex. The pattern of ibuprofen/HA complex is similar to that of pure HA, no peaks of ibuprofen detected, suggesting a thin layered structure. Fig. 2b) and 2c) for crystalline ibuprofen have been scaled down for better visualisation purposes.

As can be seen from the patterns, while both commercial and ethanol recrystallized ibuprofen specimens are highly crystalline (full match with the JCPDS database entry 32-1723), the ibuprofen/HA complex does not exhibit any reflections characteristic of ibuprofen but shows only broad reflections of a poorly crystalline HA phase. The absence of ibuprofen reflections on the XRD patterns in general can be explained by any of the following reasons: (i) amorphous or low crystalline component, (ii) particle size below 4-5 nm and (iii) highly dispersed thin layered

structure. In our case we can eliminate the amorphous phase formation as in the case of ethanol-recrystallized ibuprofen a highly crystalline material was observed (Fig. 2c), therefore the most probable explanation of the absence of the ibuprofen reflections in the ibuprofen/HA complex pattern is the presence of a well dispersed thin layer of ibuprofen or small particles.

SEM also revealed some interesting findings. Fig. 3 shows the micrographs of raw HA (a), commercial ibuprofen (b), ibuprofen after ethanol re-crystallisation (c) and ibuprofen/HA complex (d).

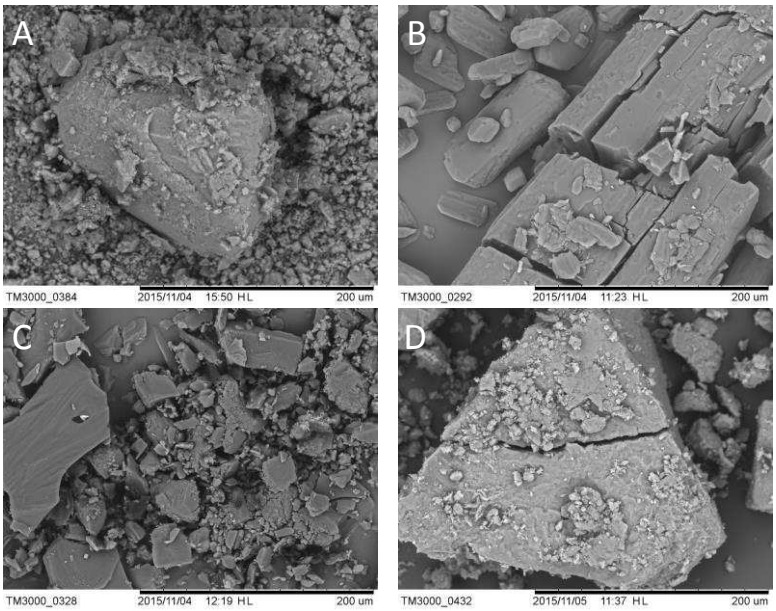

Figure 3. SEM micrographs of: a) raw hydroxyapatite, b) commercial, or as received, ibuprofen from the supplier, c) commercial ibuprofen recrystallized in ethanol, d) ibuprofen/hydroxyapatite (ibuprofen/HA) complex. Similar particle shapes and sizes were observed for as-prepared HA (a) and ibuprofen/HA complex (d).

It can be seen that raw HA consists of reasonably large agglomerates of *ca.* 200 μm and some smaller clusters of 10-20 μm. Commercial ibuprofen showed rod shaped particles of *ca.* 50-200 μm, whereas ethanol-recrystallized ibuprofen particles are random shaped with the average size

ranging from 10 to 250 μm. We do not exclude the possibility of the formation of rod-shaped particles with larger dimensions during the recrystallization of ibuprofen, as the recrystallized sample is crushed in a mortar and pestle prior to analysis, and this may not be a complete representation of the particle shape and size. However, we need to compare the ethanol treated ibuprofen specimen with the ibuprofen/HA complex that has also been ground to reach a powder form, and we believe the comparison between two SEM micrographs for these materials is valid in this case.

Another interesting feature observed during the SEM analysis was specimen destruction under the electron beam (Fig. S5). Structural damage upon irradiating the sample with the beam of electrons is a well-known phenomenon and may happen not just with organic samples [44] but also with ceramics, though at much higher accelerated voltages and current densities [45]. We decided to exploit this feature to try to visualise the presence of ibuprofen in our ibuprofen/HA complex. In other words, if the ibuprofen recrystallized in the presence of HA to form large clusters like it does in the absence of ceramics (Fig. 3c), ibuprofen particles would be damaged upon prolonged (30 sec or more) exposure to the 15 kV electron beam. However, if the ibuprofen forms a thin layer on the whole surface of the HA, it would be much harder to detect electron beam damage upon exposure. After careful inspection of the specimen of ibuprofen/HA complex under SEM at different magnifications and various irradiation times (Fig. S5) we were not able to detect any structural deformation. Thus, by using a "negative proof" approach of deliberate prolonged irradiation of the specimen with an electron beam and comparing it with bulk ibuprofen behavior in SEM under the same conditions, we demonstrated that our material is indeed a thin layered structure. While bulk ibuprofen was easily damaged by the beam, we did not find any areas of beam damage for the Ibu/HA samples, thus suggesting that no large areas of

ibuprofen clusters were formed during the synthesis, and our material is most likely a homogeneous mixture of ibuprofen and HA with the former creating a thin layer on the surface of HA. This observation is more indirect evidence of a highly dispersed thin layer of API on the surface of hydroxyapatite rather than a bi-phasic space separated API-ceramic system, thus complementing our earlier XRD findings.

Further insights into the complex formation can be obtained using ATR-FTIR spectroscopy. Fig. 4 shows the spectra of ibuprofen/HA complex (a) and ethanol treated ibuprofen (b).

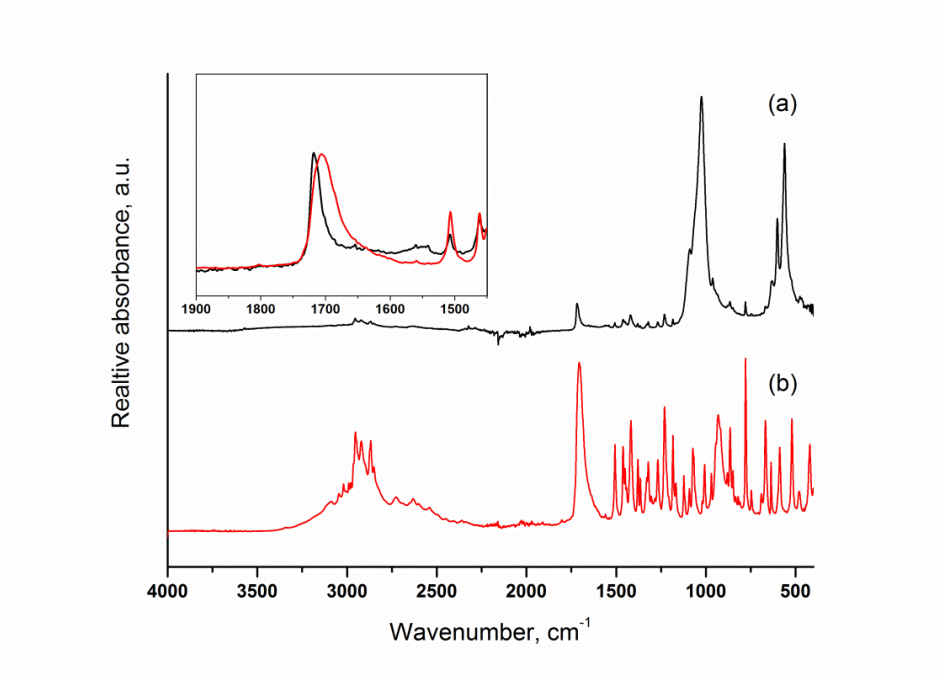

Figure 4. ATR-FTIR spectra of a) ibuprofen/HA complex and b) ibuprofen recrystallized in ethanol. Inset shows carbonyl region of ibuprofen spectra (normalised) clearly indicating the shift in frequency of ibuprofen/HA complex to higher wavenumbers (1717 cm^{-1}) compared to pure ibuprofen (1707 cm^{-1}).

The majority of active bands are in the ranges 1800 to 500 cm^{-1} and 3200 to 2400 cm^{-1} with the former assigned to carbonyl group, tertiary and quaternary carbon atoms and OH bending

vibrations, and latter to the C-H and C-C bond stretching [46]. Interestingly, overlapping of the two spectra (see inset on Fig. 4) clearly shows the shift of the ibuprofen C=O group stretching to the higher wavenumbers from the 1707 to 1717 cm^{-1}. Similar shifts have been reported in the literature and they are usually explained, yet not proved, by the hydrogen bonding between the hydroxyl group of HA and the carbonyl group of ibuprofen. However the degree of this deviation was variable from study to study, ranging from 1720 cm^{-1} [24] to 1547 cm^{-1} [23]. This large variability in literature data, as well as the lack of direct evidence on the actual nature of molecular bond interactions between ibuprofen and HA prompted us to investigate this issue in more detail.

3.3 FTIR studies of ibuprofen monomer, dimer and attached/chemisorbed species.

Firstly, we decided to evaluate the behaviour of ibuprofen in ethanol solution. It is known that ibuprofen exists in a hydrogen-bonded cyclic dimeric form that is stable in both solid and liquid phases [18]. We aimed to verify the possibility of the existence of the ibuprofen monomer in the ethanol solution as we employed this solvent for our studies. To do so we dissolved ibuprofen crystals in absolute ethanol and dropped the resulting solution onto the ATR crystal of the ATR–FTIR spectrometer and allowed it to dry naturally taking measurements at the beginning and at the end of experiment. Fig. S6a shows the IR spectrum at the zero time point measurement in the presence of ethanol, whereas Fig. S6b shows the spectrum of ibuprofen after 4 hours when the ethanol had completely evaporated (as indicated by the absence of ethanol's most active bands at 880, 1046 and 1087 cm^{-1} and a broad band between 3600 and 3000 cm^{-1}). What is immediately apparent is the presence of a broad shoulder in the region between 1760 and 1720 cm^{-1} in the spectrum corresponding to the ibuprofen dissolved in ethanol (Fig. S6a). Deconvolution of this part of the spectrum (see inset in Fig. S6) allowed us to determine the peak position of a second

species which appeared to be at *ca.* 1735 cm^{-1} and has been assigned as the C=O stretching vibration of monomer ibuprofen affected by H bonding with ethanol (further confirmed by the computational studies). Thus we have proven that ibuprofen may exist in both dimeric and monomeric forms when ethanol is present in the system.

In order to provide semi-quantitative information for the amounts of monomer and dimer in solution that will be useful for our data treatment for adsorbed species, the equilibrium constant $K_{eq,D}$ for the process $2 \times M \rightarrow D$ was determined by NMR, where M represents the monomer and D the dimer. This determination was carried out in chloroform to minimize the proton exchange and in turn line broadening, and so the visibility of the proton of the COOH group of ibuprofen involved in the dimer formation. As monomer and dimer are in fast exchange regime, the signal of the proton for the COOH group will appear as a single broad peak. Its position is dependent on the amount of monomer and dimer by the correlation: $\delta_m = \delta_M \cdot P_M + \delta_D \cdot P_D$ [47] where δ_m represents the measured average position of the proton involved in the monomer/dimer equilibrium, δ_M is an extrapolated position for the sole monomer, δ_D an extrapolate peak position for the dimer, and P_M and P_D the populations of monomer and dimer expressed in molar fraction, with the condition $P_M + P_D = 1$. Initial estimates for δ_M and δ_D were used to evaluate P_D iteratively (full details in supplementary data, Figs. S7-S13).

By using this approach a $K_{eq,D,CDCl_3} = [D]/[M]^2 = 116$ was determined, thus showing the existence of large amounts of a dimer in solution. We consider this value an upper limit with respect to the same equilibrium in ethanol. In fact, due to competing line broadening for the proton on COOH with the OH group of ethanol, it is not possible to extract this information directly in ethanol solutions. On the other hand by using this same approach it is possible to provide a crude estimate for the value of equilibrium constant for the process $M + EtOH \rightarrow M/EtOH$ by analysis

of the shift of ethanol signal in ibuprofen containing solutions. By using the same approach on peak position analysis, with $\delta_m = \delta_{EtOH} \cdot P_{EtOH} + \delta_{M/EtOH} \cdot P_{M/EtOH}$ a rough estimate of $K_{eq,EtOD} = [M/EtOH]/([M] \cdot [EtOH]) = 0.8$ was obtained, thus showing the existence of both monomer and dimer in solution.

Therefore, having assessed the presence of ibuprofen monomer in the ethanol solution, the next step was to evaluate the presence of dimer, monomer, and possible adsorbed species, in the ibuprofen/HA complex that we synthesised, using time-on-line IR spectroscopic measurements. An *in situ* experiment was carried out, using an as-prepared ibuprofen/HA complex specimen that was transferred directly from the preparation flask onto the ATR crystal of the spectrometer. Measurements were taken at various time points (from 6 to 180 min) and we did not observe any peak at 1717 cm^{-1} (as in Fig. 4 above), a band that we believe corresponds to the adsorbed monomeric ibuprofen species.

To investigate this phenomenon we performed *ex situ* measurements where the specimens were taken from the preparation flask at given time points and transferred onto the ATR crystal instead (Fig. 5).

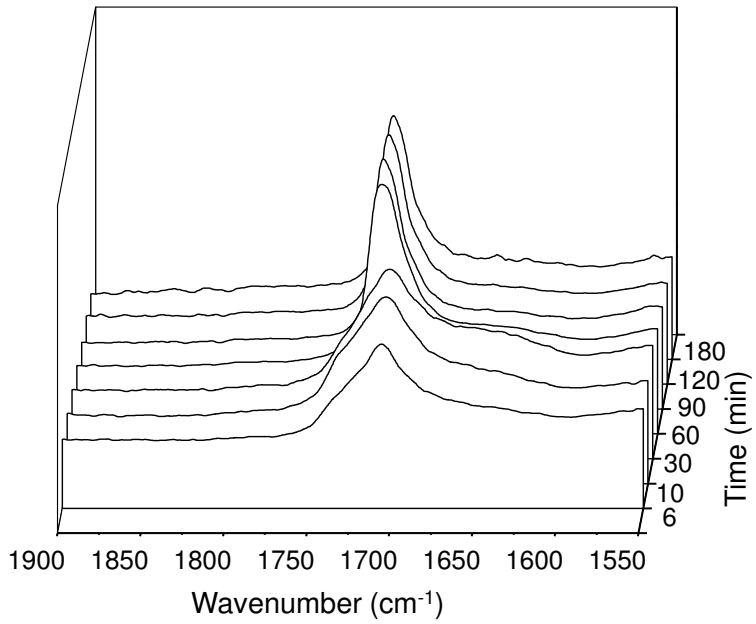

Figure 5. Kinetics of the ibuprofen/HA complex formation, *ex situ* ATR-FTIR measurements of the carbonyl region of ibuprofen between 6 and 180 min, showing the evolution of the peak assigned as attached species, and the signal decay of the dimer and monomer peaks.

This is different from the previous, *in situ*, IR experiment as in the first case the specimen is always the same across the experiment, whereas in this second case the specimens are different at every measurement time point, though still originating from the same ibuprofen/HA sample (flask). Interestingly, in the case of *ex situ* kinetic studies we were able to observe a peak at 1717 cm^{-1} instead. This suggests that keeping a specimen between the force applicator and the ATR crystal for the whole duration of the in situ experiment (180 min) prevents the formation of the adsorbed species, leading only to the re-crystallisation of the ibuprofen dimer.

3.4 Mechanistic studies and molecular modelling.

The data gathered using *ex situ* time-on-line IR studies for the ibuprofen/HA complex prompted us to investigate and describe a possible mechanism for the inter-molecular complex

formation by using a combination of computational studies, as well as FTIR and Raman spectroscopies.

Computational studies were carried out using density functional theory and a B3LYP functional, using 6-311G(d,p) basis set for all other atoms. Our model considers the energetics of an ibuprofen monomer versus a more stable dimeric species and the interaction that this monomer can have with a hydroxyapatite adsorption site.

3.4.1 Energetics and structures of ibuprofen monomer and dimer.

Ibuprofen is a molecule that can exist in several conformers. By using a B3LYP/6-31G(d) level of theory, De Cararvalho and co-workers identified eight stable minima [46]. Of these conformers the most stable and the one best matching IR data was a structure presenting the carboxyl and isobutyl groups of the ibuprofen molecule on opposite sides with respect to the plane of the benzene ring. Employing this structural element as a starting point, we optimized this structure using a higher level of theory for structure optimization, B3LYP/6-311G(d,p), and obtained the structure reported in Figures 6a and 6b. This has been used as a model for the formation of an ibuprofen dimer, as well as ibuprofen/HA interactions in our study.

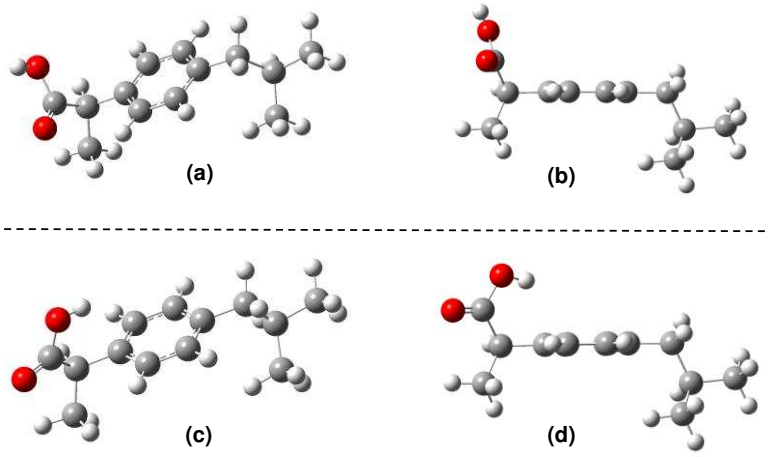

Figure 6. Ibuprofen structure optimized using a DFT/B3LYP/6-311G(d,p) level of theory. (a) and (b) absolute minimum with: (a) ibuprofen view from top highlighting the carboxyl group, and (b) ibuprofen view from side to highlight the relative position of carbonyl and isopropyl groups with respect to the benzene ring. (c) and (d) relative minimum for a conformer obtained by rotation of the carbonyl group along a C-C axis from structure (a). For this second structure: (c) view from top highlighting the rotation of the carbonyl group, and (d) view from a side with respect to the benzene ring plane. Note the orientation of the hydroxyl group with the H atom pointing to the benzene ring, underlying an intramolecular hydrogen bond. Colour code: (red atoms) oxygen, (grey atoms) carbon, (white atoms) hydrogen.

For completeness, we should mention that we identified a further minimum (Fig. 6c and 6d) close in energy to the previous one, with an energy gap of + 15 kJ mol^{-1}. This energy gap is reasonably small and the two species might both exist in solution. We think this second minimum exists by virtue of an intra-molecular hydrogen bond between the H atom of the hydroxyl group and the benzene ring [48] (Fig. 6d). However, as this conformer is less stable, and it would not be able to form a dimer because of the orientation of the hydroxyl group pointing to the benzene ring, it will not be considered further in our discussion.

Using the conformer in Fig. 6a and 6b we first determined the structure of an ibuprofen dimer. In principle, two dimeric forms can be postulated: a *cis* form with the carbon skeletons of the two ibuprofen molecules facing each other, or a *trans* form where the carbon skeletons of the two molecules are in the opposite direction with respect to the plane identified by the carboxylic groups of ibuprofen. In this study only the *trans* dimer has been considered as it is the most stable and its existence has been proved in solid state [18]. Using our model, the *trans* dimer (Fig. S14) has a stabilization energy with respect to two isolated molecules of ibuprofen of -69

kJ mol^{-1}. This indicates a strong H-bond interaction between the OH and CO groups of the carboxyl unit of a molecule of ibuprofen with the CO and OH groups respectively of another molecule of ibuprofen (Fig. S14).

Conversely, it also shows that the process of dissociation of a dimer to two units of monomer is not spontaneous. However, as in our experiments ibuprofen is dissolved in ethanol, and we detected the existence of an IR band at 1735 cm^{-1} (see section 3.3) when both ibuprofen and ethanol are present, we can assume that this solvent promotes the dimer dissociation into two monomer units. That is the formation of an ibuprofen/ethanol complex in solution via the reaction: D + 2EtOH $\rightarrow$ 2 M/EtOH (where D and M stand for dimer and monomer respectively). A stable hydrogen-bonded M/EtOH complex was identified (Fig. S15) and the energetics of this dissociation reaction assisted by ethanol was calculated to be -29 kJ mol^{-1} and thus favoured.

It should be noted that our IR data identify a peak at 1735 cm^{-1} that is observed in the presence of ethanol only. With our data we think we can assign this peak to an ibuprofen/ethanol complex as expected in the dissolution process.

3.4.2 Hydroxyapatite adsorption site.

In order to mimic hydroxyapatite and ibuprofen interaction, an adsorption site was built. This site was constructed by using a simplified, yet useful, model comprising the most distinct features of hydroxyapatite in place of a whole hydroxyapatite crystal. These features are: the presence of a phosphate group bound to a calcium atom presenting two hydroxyl groups (Fig. S16).

In order to validate whether this neutral HA fragment is representative for our studies, we calculated the position of IR bands for: stretching and bending motions of the phosphate group, and for the libration motion of the OH groups (which are also bound to a single Ca centre in a

HA crystal). Our model calculates these vibrations at: 1036, 411, and 608 cm^{-1} respectively. Experimental values for these same vibrations, are: 1020, 443, and 632 cm^{-1} [49]. Taking into account that our simplified model does not include lattice parameters, the calculated wavenumber values are in good agreement with experimental data, and as such we consider it as a good platform for the investigation of ibuprofen and hydroxyapatite interactions.

3.4.3 Ibuprofen and hydroxyapatite interactions.

From the ibuprofen and HA structures described in sections 3.4.1 and 3.4.2 (and Figs 6 and S16) an adsorption complex between ibuprofen and hydroxyapatite was built. A stable minimum with a large stabilization energy of -133 kJ mol^{-1} was found (Fig. S17).

This minimum presents a hydrogen bond interaction between ibuprofen and HA. However, and quite interestingly, this H-bond interaction occurs between the OH group of the carboxyl function of ibuprofen ($HO_{ibuprofen}$) and the hydroxyl groups of the hydroxyapatite bound to Ca ($HO_{apatite}$) in a $HO_{apatite}$---$HO_{ibuprofen}$ interaction. That is, this bond does not involve an H-bond between the CO group of ibuprofen ($CO_{ibuprofen}$) and the OH group of the hydroxyapatite ($HO_{apatite}$) in a $CO_{ibuprofen}$---$HO_{apatite}$ interaction, but the carbonyl group appears to interact with the apatite via a Ca centre, as a $CO_{ibuprofen}$---$Ca_{apatite}$ instead. As such two anchoring points for ibuprofen are present via $HO_{apatite}$ and $Ca_{apatite}$ centres.

In the other words, an H-bond is present and as such fits current tentative explanations of ibuprofen and HA interactions [23]; however, in our case this is an $HO_{apatite}$---$HO_{ibuprofen}$ hydrogen bond interaction, and not a $CO_{ibuprofen}$---$HO_{apatite}$ H-bond interaction [23]. Furthermore, our model also suggests that changes in vibrational frequencies of the C=O group of ibuprofen are also due to the existence of a non H-bond, $CO_{ibuprofen}$---$Ca_{apatite}$ interaction.

For this complex we calculated a C=O vibrational frequency of 1694 cm^{-1}. This correctly predicts a red shift of about 50 cm^{-1} with respect to an isolated monomeric species (expected at 1746 cm^{-1}). However, our level of theory does not allow an unambiguous assignment of IR bands from the spectra as the dimer is also calculated in the 1694 cm^{-1} region. In this context though, it is worth noting that such an interaction is not unusual between a carboxyl group and a metal centre and it has been observed in the case of species containing Zn [50] where the carboxyl group binds via the carbonyl unit in a mono-dentate manner, and it might be operating also in our case.

Raman scattering is sensitive to changes in polarizability [51] and has therefore different selection rules compared to IR absorption, and the two techniques can complement each other. For this specific case we applied Raman spectroscopy to have a wide splitting between the Raman active symmetric C=O stretching frequency of the dimer, and the C=O stretching vibration of the adsorbed species. The C=O stretching vibrations of the dimer split into the symmetric, Raman active vibration at lower wavenumber, and the antisymmetric, IR active vibration at higher wavenumber. Whereas in the IR spectrum, the antisymmetric C=O stretching of the dimer partially overlaps with the C=O stretching vibration of the adsorbed monomer, in the Raman spectrum, the vibrations are much more separated making an assignment and interpretation less ambiguous. Raman spectra for pure ibuprofen, ibuprofen in the presence of ethanol, and a sample from an ibuprofen, ethanol and HA mixture after drying, are reported Fig. 7.

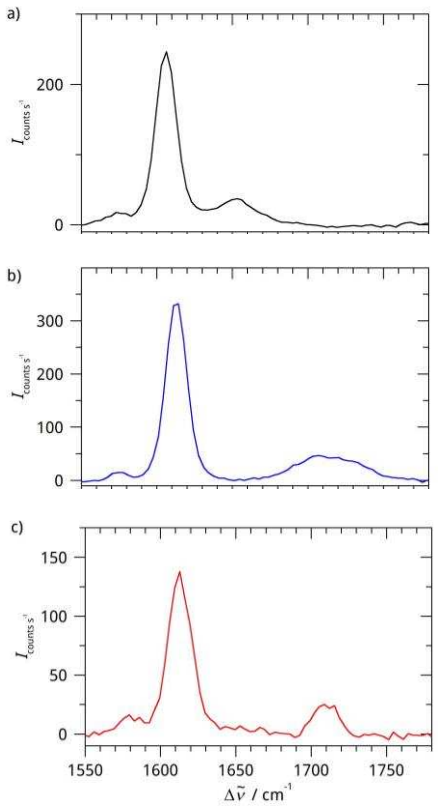

Figure 7. Raman spectra of (a) pure ibuprofen powder, (b) ibuprofen-ethanol solution and (c) ibuprofen-loaded H-apatite (dry). The most intense band at *ca.* 1610 cm^{-1}, observed in all spectra, is a C-C stretching vibration of the aryl ring. The band at 1652 cm^{-1} observed in spectrum (a) is the symmetric stretching of the C=O bond in the dimer. The broad band in the region 1700-1730 cm^{-1} in spectrum (b) is for a C=O stretching of ibuprofen in an ibuprofen/ethanol complex. The band at 1710 cm^{-1} for spectrum (c) arises from the C=O stretching of ibuprofen in an ibuprofen/HA complex.

The most intense peak of this set of spectra is centered at *ca.* 1610 cm^{-1} and corresponds to the vibration of the C-C bond of the benzyl ring. The weaker peak at 1652 cm^{-1} in spectrum (a) corresponds to the symmetric C=O stretching vibration of an ibuprofen dimer [52]. The presence of this peak has to be expected in a sample of pure ibuprofen (Fig. 7a) because the dimer is the most stable species in solid form (vide supra).

When some ethanol is added to the sample (Fig. 7b) the 1652 cm^{-1} dimer band disappears and a new and broad peak in the region 1700-1730 cm^{-1} appears. We ascribe this signal to a C=O stretching vibration of monomer ibuprofen affected by H bonding with ethanol. In the case of ibuprofen/HA complex sample (Fig. 7c) we can note the presence of a sharper peak at *ca.* 1710 cm^{-1} that we assign to C=O stretching of an ibuprofen monomer adsorbed to HA, possibly via a C=O---Ca interaction as described above. In this spectrum, the dimer peak at 1652 cm^{-1} has disappeared, showing that in this sample ibuprofen is likely not in the dimer configuration anymore, but mainly bonded to HA. The small but significant shift of the C-C stretching at 1610 cm^{-1} moving from spectrum (a) to spectra (b) and (c), reflects a change from a dimer to a monomer.

Considering these assignments, a summary of the stabilization energies of ibuprofen with respect to dimer, monomer/EtOH, and monomer/HA, that will be useful of our reasoning for the next sections, is reported below (Fig. 8, Table S1):

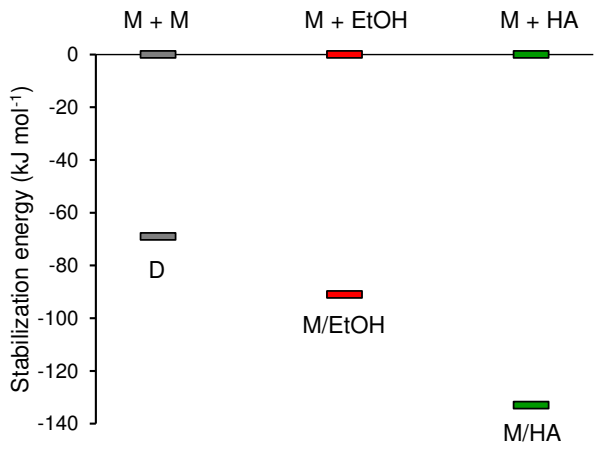

Figure 8. Energy diagram summarizing the stabilization energies for dimer or complexes formation from a monomer of ibuprofen. The symbol '+' stands for two isolated molecules or fragments, the symbol '/' stands for a complex formation. M = ibuprofen monomer, D = dimer, EtOH = ethanol, HA = hydroxyapatite.

From the energy diagram it is possible to observe that any interaction of the monomer with another monomer, ethanol or HA is always a favourable process. However, the most energetically stable interaction is the one between a monomer of ibuprofen and hydroxyapatite, thus suggesting the formation of an adsorbed species. In addition, the formation of an ibuprofen/ethanol complex is also favoured with respect to the formation of an ibuprofen dimer from two independent monomeric units, and thus supporting a dissolution process and the formation of a monomer under our conditions, as detected in IR (Fig. S5 and at 1735 cm^{-1}), and importantly the disappearance at 1652 cm^{-1} from Raman spectra (from a dimer) when ethanol is added (Fig. 7b) and the formation of a new band in the region of 1700-1730 cm^{-1}.

3.4.4 Kinetics of the adsorption of ibuprofen to the surface of hydroxyapatite.

Having ascertained the presence of an adsorbed ibuprofen species to HA, and with this species possibly presenting a hydrogen bond $HO_{apatite}$---$HO_{ibuprofen}$, and a $CO_{ibuprofen}$---$Ca_{apatite}$ interaction, we carried out a kinetic study in order to gain an in-depth knowledge of the adsorption process.

From the spectra reported in section 3.3, it is possible to observe a decay of the signal for a M/EtOH species, an increase of an adsorbed ibuprofen species on the HA surface, here denoted M/HA, and a nearly constant signal for the ibuprofen in dimeric form, here denoted as D. The signal intensities are reported in Fig. 9.

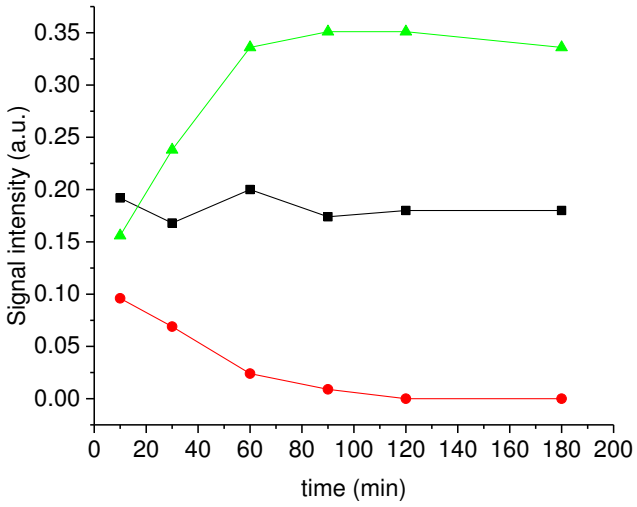

Figure 9. Signal intensity evolution (from ATR-FTIR) against time for: (●) ibuprofen monomer (vide infra), (■) ibuprofen dimer, and (▲) monomer adsorbed over HA surface.

The nearly constant signal for the bulk ibuprofen dimer D can be easily explained with the working principle of the ATR-FTIR method (see section 3.1) [36]. This technique is often referred as a surface method, but with a penetration depth of a few microns. Therefore with respect to ibuprofen present in layers like M/EtOH or M/HA, the ibuprofen presenting a dimer D appears an in large excess, and therefore no change in its intensity occurs.

A M/EtOH complex can form an adsorbed species or evolve to a dimer. The energetics for these processes are reported here (per molecule of ibuprofen), in eqs 1-2.

$M/EtOH + HA \rightarrow M/HA + EtOH \quad \Delta E = -84 \text{ kJ mol}^{-1}$ (eq.1)

$2 \times M/EtOH \rightarrow D + 2 \times EtOH \quad \Delta E = +29 \text{ kJ mol}^{-1}$ (eq.2)

It should be noted that if ethanol is accounted into the process, whereas the adsorption of an ibuprofen molecule is a favourable process (eq. 1 and eq. 2), the formation of a dimer in the presence of ethanol (eq. 2) is now an unfavourable process presenting a small, yet positive, ΔE of $+29 \text{ kJ mol}^{-1}$. This was not the case if the dimer formation was considered without the presence

of ethanol (see section 3.4.1), where a stabilization energy of – 69 kJ mol^{-1} was calculated instead.

As a consequence, these data would suggest that the increase in signal that we observe in spectra in Fig. 5 is due to a process involving the evolution of a M/EtOH species to an adsorbed one, M/HA, a process now favoured with respect to the formation of a dimer.

In order to experimentally discriminate between the evolution of a monomer M or M/EtOH species to an adsorbed Mads or M/HA against a dimeric species D, we applied a kinetic analysis to the signal decay. In fact, for a monomer that evolves to an adsorbed species, either $M \rightarrow M_{ads}$ or M/EtOH + HA $\rightarrow$ M/HA +EtOH, this would imply a first order decay of the signal I of M/EtOH and a kinetics equal to (eq.3):

$$I_t = I_0 \cdot e^{-kt} \quad \text{(eq.3)}$$

where I_t is the intensity of the IR signal (absorbance) at the time *t, k* is the kinetic constant of the decay process, and I_0 is the intensity of the signal at the start of the measurement.

If the monomer M or M/EtOH evolves to a dimer (D = 2M) instead (or 2 × M/EtOH $\rightarrow$ D + 2EtOH), this implies the consumption of two molecules of monomer (2M $\rightarrow$ D) and in turn a second order kinetics instead. In this case the process is described by the equation:

$$I_t = \frac{I_0}{1 + ktI_0} \quad \text{(eq. 4)}$$

Both these models were used to fit the signal decay of the monomeric species (Fig. S18). It is possible to observe that a first order kinetics (Fig. S18a) fits the data well for the decay of the monomeric species, unlike a second order model (Fig. S18b), with values of R^2 equal to 0.985 and 0.894 respectively. We can then conclude that, based on both calculated stability and fitted kinetics, the decay of signal from the monomeric species M/EtOH is consistent with its evolution

to an adsorbed species over the HA surface: $M \rightarrow M_{ads}$, for a process: M/EtOH + HA $\rightarrow$ M/HA + EtOH.

The same principle has been applied for the growth of the signal of the adsorbed species. From the raw data (Fig. 9) it also appears that the bare growth of the adsorbed species is between two and three times the decay of the monomeric species. However, as the signal is related to the absorbance A by the Beer-Lambert law $A = \varepsilon bc$ the signal is also a function of the intrinsic extinction coefficient epsilon. By using our level of theory the stretching of the carbonyl group for an adsorbed species is *ca.* two times more intense than the intensity of the signal for an isolated monomer. If we apply this as a correction factor to the growth of the adsorbed species, the kinetics of the growth for the adsorbed species is nearly identical to the kinetics of decay of the monomer (Fig. S18).

In order to further corroborate these data, we estimated the equilibrium constant $K_{eq,Ads}$ for the process $M_{ads} \rightarrow M_{ads}$, by analyzing the decay of the free monomer and the growth of the adsorbed species. We estimated a $K_{eq,Ads} = [M_{ads}]/[M_{ads}] = 39$. It should be noted that this value is in the same order of magnitude as the estimated equilibrium constant for the dimer formation in ethanol. We think this is another factor that contributes to our capability to detect and monitor the evolution of a free ibuprofen species to an attached species over the HA surface.

In summary, the adsorption process of an ibuprofen molecule to a site on HA can be schematized as follow:

$D + 2\ EtOH \rightarrow 2 \times M/EtOH\ \Delta E = -29\ kJ\ mol^{-1}$ (eq. 5)

$2 \times (M/EtOH + HA \rightarrow M/HA + EtOH)\ \ \Delta E = 2 \times (-84\ kJ\ mol^{-1}) = -168\ kJ\ mol^{-1}$ (eq. 6)

Net equation:

$D + 2\ HA \rightarrow 2 \times M/HA\ \Delta E = -197\ kJ\ mol^{-1}$ (eq. 7)

That is, the adsorption of a monomeric ibuprofen species to an adsorption site of HA is a largely energetically favourable process that occurs in two steps: the dissociation of the ibuprofen dimer to a monomer mediated by ethanol, and the adsorption process to the HA surface via a first order kinetics.

3.5 Dissolution studies.

Finally, we decided to verify how the adsorption of ibuprofen on the surface of hydroxyapatite will influence the drug release properties. Fig. 10 shows the drug release profiles of pure ibuprofen (as a control), a physical mixture of ibuprofen and HA, and ibuprofen/HA complex that we proved to be made of a hydrogen bonded API monomer weakly attached to the surface of HA. Fig. 11 demonstrates that the drug release of physical mixture is similar to that of a pure ibuprofen, whereas the drug release rate for the ibuprofen/HA complex is statistically slower at the initial time points (between 5 and 180 min) but then equalises by the 4 hour measurement. There have been some reports studying the correlation between the structure and/or porosity of hydroxyapatite vs. ibuprofen release [23, 24]. In these studies, the porosity of the system significantly increases the drug retention time, whereas in our case we observe only a slight delay in the drug release during the first hour. This could possibly be explained by the fact that the main cause of the retardation of ibuprofen release is due to weak intermolecular bonding between the API and the carrier, and not the geometry of the HA. The intense drug release at the early time points of the dissolution is normally associated with the concentration gradients on the surface where diffusion pathways are short, followed by the decrease of the drug release rate due to the increase in the diffusion pathways from the bulk. Such formulations are referred to as

diffusion-controlled drug delivery system, and the kinetics is based on the known cylindrical geometry of the tablets and Fick's second law of diffusion [24]. In our case, however, we did not produce tablets, and therefore ibuprofen that formed a thin layer on the surface of the HA powder is readily released mostly from the surface rather than the bulk, thus suggesting that the profile observed in Fig. 10 is not fully diffusion controlled.

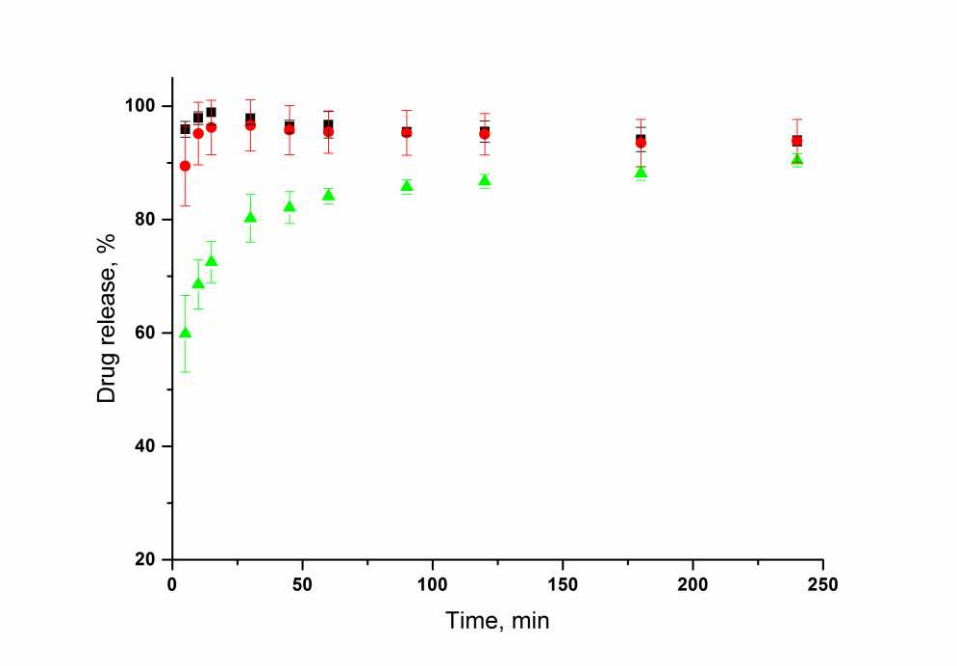

Figure 10. Drug release profile of: as received ibuprofen (■), physical mixture of ibuprofen and hydroxyapatite (●) and hydrogen bonded ibuprofen-hydroxyapatite complex (ibuprofen/HA) (▲). Slower release rate for the ibuprofen/HA complex can be clearly noted, whereas raw ibuprofen and a physical mixture of ibuprofen and HA present similar dissolution rates.

We relate this slower, and desirable, drug release to the adsorption of the API compared to the bi-phasic physical mixture where the two components are not bonded to one another, thus proving that the intra-molecular bonding effect between the API and a carrier is an important factor when designing materials with controlled drug release properties. The majority of the studies on combining ceramics and anti-inflammatories concentrate their attention on prolonged

drug release, whereas for the treatment of arthritic patients a “burst” drug release may be required at a point of need followed by a prolonged drug release afterwards [53]. Our study suggests that when ibuprofen and HA form a hydrogen-bonded complex it may be more difficult to obtain an immediate release due to an API-carrier interaction, in turn impeding design of materials with dual properties when using the method of dissolving and recrystallising drug in the presence of a ceramic carrier.

4. Conclusions

In this study, we elucidated the mechanism of the ibuprofen adsorption onto the surface of nano-hydroxyapatite and its effects on the drug dissolution rate, explaining earlier findings on the shift of the FTIR signal of the carbonyl group of the API in the presence of ceramics. Herein, using an array of characterisation tools we demonstrated that when synthesising an ibuprofen/ceramic complex, a hydrogen bonding occurs between the carbonyl group of the API and a calcium centre of hydroxyapatite. The process of surface-attachment follows the steps: (i) ibuprofen dimer partial dissolution in a solvent, (ii) formation of a monomer/solvent complex from a dimer, (iii) subsequent preferential attachment of the ibuprofen monomer to the hydroxyapatite. The latter is represented by a hydrogen bond between the hydroxyl group of ibuprofen and one of the hydroxyl groups of the hydroxyapatite, along with an interaction between the carbonyl group of ibuprofen and a calcium centre of HA. The formation of this complex occurs by means of a first order kinetics.

Furthermore, we have also demonstrated the influence of such non-covalent bonding on the release/dissolution rate of the drug. Through investigation of the behaviour of the intramolecular bonded system ibuprofen-hydroxyapatite under physiological conditions (phosphate buffer) and

comparing it with the bi-phasic mixture of the two components we have shown that the initial API release rate from the complex is influenced by the hydrogen bond induced attachment of the ibuprofen to the surface of nano-hydroxyapatite. On a wider perspective, we believe the results of this work will help to understand the effect of hydrogen-bonding on the attachment of the APIs to the surface of the drug carrier and its contribution to the dissolution profile of the system.

5. Acknowledgments

Authors would like to acknowledge funding support from EPSRC (EP/L027011/1, EP/K029592/1). This research was performed in part at the MIDAS Facility, at the University of Sheffield, which was established with support from the Department of Energy and Climate Change.

ASSOCIATED CONTENT

Supporting Information. The Supporting Information is available free of charge on the ACS Publications website.

AUTHOR INFORMATION

Corresponding Author

* Anant Paradkar Centre for Pharmaceutical Engineering Science, University of Bradford, Bradford, BD7 1DP, UK. Phone: +44 (0) 1274 233900, a.paradkar1@bradford.ac.uk

Author Contributions

The manuscript was written through contributions of all authors. All authors have given approval to the final version of the manuscript.

REFERENCES

[1] Vallet-Regi, M; Gonzalez-Calbet, J. Calcium phosphates as substitution of bone tissues. *J. Prog. Solid State Chem*. **2004**, *32*, 1-31.

[2] Ogilvie, A.; Frank, R.M.; Benqué, E.P.; Gineste, M.; Heughebaert, M.; Hemmerle, J. The biocompatibility of hydroxyapatite implanted in the human periodontium. *J. Periodontal Res.* **1987**, *22*, 270-283.

[3] Deville, S.; Saiz, E.; Tomsia, A. P. Freeze casting of hydroxyapatite scaffolds for bone tissue engineering. *Biomaterials* **2006**, *27*, 5480-5489.

[4] Hruschka, V.; Tangl, S.; Ryabenkova, Y.; Heimel, P.; Barnewitz, D.; Möbus, G.; Keibl, C.; Ferguson, J.; Quadros, P.; Miller, C.; Goodchild, R.; Austin, W.; Redl, H.; Nau, T. Comparison of nanoparticular hydroxyapatite pastes of different particle content and size in a novel scapula defect model. *Sci. Rep*. **2017**, *7*, 43425; doi: 10.1038/srep43425.

[5] Wu, G.J.; Zhou, L.Z.; Wang, K.W.; Chen, F.; Sun, Y.; Duan, Y.R.; Zhu Y. J.; Gu, H. C. Hydroxylapatite nanorods: An efficient and promising carrier for gene transfection. *J. Colloid Interface Sci.* **2010**, *345*, 427-432.

[6] Ma, M.Y.; Zhu, Y.J.; Li, L.; Cao, S.W. Nanostructured porous hollow ellipsoidal capsules of hydroxyapatite and calcium silicate: preparation and application in drug delivery. *J. Mater. Chem.* **2008**, *18*, 2722-2727.

[7] Long, T.; Guo, Y.-P.; Liu, Y.-Z.; Zhu, Z.-A. Hierarchically nanostructured mesoporous carbonated hydroxyapatite microspheres for drug delivery systems with high drug-loading capacity. *RSC Adv.* **2013**, *3*, 24169-24176.

[8] Ueno, Y.; Futagawa, H.; Takagi, Y.; Ueno, A.; Mizushima, Y. Drug-incorporating calcium carbonate nanoparticles for a new delivery system. *J. Control. Release* **2005**, *103*, 93-98.

[9] Wang, C.; He, C.; Tong, Z.; Liu, X.; Ren, B.; Zeng, F. Combination of adsorption by porous CaCO3 microparticles and encapsulation by polyelectrolyte multilayer films for sustained drug delivery. *Int. J. Pharm.* **2006**, *308*, 160-167.

[10] Zhou, J.; Horev, B.; Hwang, G.; Klein, M.I.; Koob, H.; Benoit, D.S.W. Characterization and optimization of pH-responsive polymer nanoparticles for drug delivery to oral biofilms. *J. Mater. Chem. B* **2016**, *4*, 3075-3085.

[11] Ashley, G.W.; Henise, J.; Reid, R.; Santi, D.V. Hydrogel drug delivery system with predictable and tunable drug release and degradation rates. *Proc. Natl. Acad. Sci. U S A.* **2013**, *110*, 2318-2323.

[12] Pham, H. H.; Luo, P.; Génin, F.; Dash, A. K. Synthesis and characterization of hydroxyapatite-ciprofloxacin delivery systems by precipitation and spray drying technique. *AAPS PharmSciTech* **2002**, *3*, 1-9.

[13] Joosten, U.; Joist, A.; Gosheger, G.; Liljenqvist, U.; Brandt, B.; von Eiff, C. Effectiveness of hydroxyapatite-vancomycin bone cement in the treatment of Staphylococcus aureus induced chronic osteomyelitis. *Biomaterials* **2005**, *26*, 5251-5258.

[14] Jafari, S.; Maleki-Dizaji, N.; Barar, J.; Barzegar-Jalali, M.; Rameshrad, M.; Adibki, K. Physicochemical characterization and in vivo evaluation of triamcinolone acetonide-loaded hydroxyapatite nanocomposites for treatment of rheumatoid arthritis. *J. Colloid. Surface B* **2016**, *140*, 223-232.

[15] Felson, D.T.; Lawrence, R.C.; Dieppe, P.A.; Hirsch, R.; Helmic, C.G.; Jordan J.M. et al, Osteoarthritis: New Insights. Part 1: The Disease and Its Risk Factors. *Ann. Intern. Med.* **2000**, *133*, 635-646.

[16] Araujo, C.G.; Fernandez Gonzalez, J.; Tonino, A. Rheumatoid arthritis and hydroxyapatite-coated hip prostheses. *J. Arthroplasty* **1998**, *13*, 660-667.

[17] Boureau, F.; Schneid, H.; Zeghari, N.; Wall, R.; Bourgeois, P. The IPSO study: ibuprofen, paracetamol study in osteoarthritis. A randomised comparative clinical study comparing the efficacy and safety of ibuprofen and paracetamol analgesic treatment of osteoarthritis of the knee or hip. *Ann. Rheum. Dis.* **2004**, *63*, 1028-1034.

[18] Lerdkanchanaporn, S.; Dollimore, D. A thermal analysis study of ascorbic acid and its pharmaceutical formulations. *J. Therm. Anal. Calorim.* **1997**, *49*, 879−886.

[19] Smeyers, Y.G.; Cuéllare-Rodriguez, S.; Galvez-Ruano, E.; Arias-Pérez, M.S. Conformational analysis of some α-phenylpropionic acids with anti-inflammatory activity. *J. Pharm. Sci.* **1985**, *74*, 47-49.

[20] Kierys, A.; Grochowicz, M.; Kosik, P. Fabrication of porous hollow γ-Al2O3 nanofibers by facile electrospinning and its application for water remediation. *Micropor. Mesopor. Mater.* **2015**, *217*, 133-140.

[21] Qi, C.; Zhu, Y.-J.; Lu, B.-Q.; Zhao, X.-Y.; Zhao, J.; Chen, F. Hydroxyapatite nanosheet-assembled porous hollow microspheres: DNA-templated hydrothermal synthesis, drug delivery and protein adsorption. *J. Mater. Chem.* **2012**, *22*, 22642-22650.

[22] Melville, A.J.; Rodríguez-Lorenzo, L. M.; Forsythe, J.S. Effects of calcination temperature on the drug delivery behaviour of Ibuprofen from hydroxyapatite powders. *J. Mater. Sci.-Mater. Med.* **2008**, *19*, 1187-1195.

[23] Sambudia, N.S.; Chob, S.; Cho, K. Porous hollow hydroxyapatite microspheres synthesized by spray pyrolysis using a microalga template: preparation, drug delivery, and bioactivity. *RSC Adv.* **2016**, *6*, 43041-43048.

[24] Öner, M.; Yetiz, E.; Ay, E.; Uysal, U. Ibuprofen release from porous hydroxyapatite tablets. *Ceram. Int.* **2011**, *37*, 2117-2125.

[25] Kumar, R.; Prakash, K.H.; Cheang, P.; Khor, K.A. Temperature driven morphological changes of chemically precipitated hydroxyapatite nanoparticles. *Langmuir* **2004**, *20*, 5196-5200.

[26] Cullity, B.D.; Stock S.R. in *Elements of X-Ray Diffraction*, Prentice-Hall Inc, Upper Saddle River, 3rd edn, **2001**, p. 236.

[27] Mohr, C.; Spenser, C.L.; Hippler, M. Inexpensive raman spectrometer for undergraduate and graduate experiments and research. *J. Chem. Educ.* **2010**, *87*, 326-330.

[28] www.webbook.nist.gov; accessed 23/3/2016.

[29] Frisch, M. J.; Trucks, G. W.; Schlegel, H. B.; Scuseria, G. E.; Robb, M. A.; Cheeseman, J. R.; Scalmani, G.; Barone, V.; Mennucci, B.; Petersson, G. A.; Nakatsuji, H.; Caricato, M.; Li, X.; Hratchian, H. P.; Izmaylov, A. F.; Bloino, J.; Zheng, G.; Sonnenberg, J. L.; Hada, M.; Ehara, M.; Toyota, K.; Fukuda, R.; Hasegawa, J.; Ishida, M.; Nakajima, T.; Honda, Y.; Kitao, O.; Nakai, H.; Vreven, T.; Montgomery, J. A., Jr.; Peralta, J. E.; Ogliaro, F.; Bearpark, M. J.; Heyd,

J.; Brothers, E. N.; Kudin, K. N.; Staroverov, V. N.; Kobayashi, R.; Normand, J.; Raghavachari, K.; Rendell, A. P.; Burant, J. C.; Iyengar, S. S.; Tomasi, J.; Cossi, M.; Rega, N.; Millam, N. J.; Klene, M.; Knox, J. E.; Cross, J. B.; Bakken, V.; Adamo, C.; Jaramillo, J.; Gomperts, R.; Stratmann, R. E.; Yazyev, O.; Austin, A. J.; Cammi, R.; Pomelli, C.; Ochterski, J. W.; Martin, R. L.; Morokuma, K.; Zakrzewski, V. G.; Voth, G. A.; Salvador, P.; Dannenberg, J. J.; Dapprich, S.; Daniels, A. D.; Farkas, O.; Foresman, J. B.; Ortiz, J. V.; Cioslowski, J.; Fox, D. J. *Gaussian 09, Revision D.01*; Gaussian, Inc.: Wallingford, CT, **2009**.

[30] Stephens, P.; Devlin, F.; Chabalowski, C.; Frisch. M.J. Ab Initio calculation of vibrational absorption and circular dichroism spectra using density functional force fields *J. Phys. Chem.* **1993**, *98*, 11623–11627.

[31] Narbutt, J.; Oziminski, W.P. Selectivity of bis-triazinyl bipyridine ligands for americium(III) in Am/Eu separation by solvent extraction. Part 1. Quantum mechanical study on the structures of BTBP complexes and on the energy of the separation. *Dalton Trans.* **2012**, *41*, 14416–14424.

[32] Ahrens, T.; Ahrens, M.; Braun, T.; Braun, B.; Herrmann, R. Synthesis of a rhodium(I) germyl complex: a useful tool for C–H and C–F bond activation reactions. *Dalton Trans.* **2016**, *45*, 4716–4728.

[33] Andersson, M.P.; Uvdal, P. New scale factors for harmonic vibrational frequencies using the B3LYP density functional method with the triple-ζ basis set 6-311+G(d,p). *J. Phys. Chem. A* **2005**, *109*, 2937–2941.

[34] Liao, C.-J.; Lin, F.-H.; Chen, K.-S.; Sun, J.-S. Thermal decomposition and reconstitution of hydroxyapatite in air atmosphere. *Biomaterials* **1999**, *20*, 1807-1813.

[35] Gulley-Stahl, H.; Hogan, P.A.; Schmidt, W.L.; Wall, S.J.; Buhrlage, A.; Bullen, H.A. Surface complexation of catechol to metal oxides: an ATR-FTIR, adsorption, and dissolution Study. *Environ. Sci. Technol.* **2010**, *44*, 4116–4121.

[36] Jabbari, E.; Wisniewski, N.; Peppas, N.A. Evidence of mucoadhesion by chain interpenetration at a poly(acrylic acid)/mucin interface using ATR-FTIR spectroscopy. *J. Control. Release* **1993**, *26*, 99-108.

[37] Huang, L.Y.; Xu, K.W.; Lu, J. Bone healing in porous implants. An experiment in sheep. *J. Mater. Sci.-Mater. Med.* **2000**, *11*, 667-673.

[38] Lim, G.K.; Wang, J .; Ng, S.C.; Gan, L.M. Nanosized hydroxyapatite powders from microemulsions and emulsions stabilized by a biodegradable surfactant. *J. Mater. Chem.* **1999**, *9*, 1635-1639.

[39] Gibson, I.R.; Rehman, I.; Best, S.M.; Bonfield, W. Characterization of the transformation from calcium-deficient apatite to beta-tricalcium phosphate. *J. Mater. Sci.-Mater. Med.* **2000**, *11*, 799-804.

[40] Viswanath, B.; Ravishankar, N. Controlled synthesis of plate-shaped hydroxyapatite and implications for the morphology of the apatite phase in bone. *Biomaterials* **2008**, *29*, 4855-4863.

[41] Gibson, I.R.; Bonfield, W. Novel synthesis and characterization of an AB-type carbonate-substituted hydroxyapatite. *J. Biomed. Mater. Res.* **2002**, *59*, 697-708.

[42] Ibrahim, D.M.; Mostafa, A.A.; Korowash, S.I. Chemical characterization of some substituted hydroxyapatites. *Chem. Cent. J.* **2011**, *5*, 74.

[43] Chevalier, E.; Viana, M.; Cazalbou, S.; Makein, L.; Dubois, J.; Chulia, D. Ibuprofen-loaded calcium phosphate granules: Combination of innovative characterization methods to relate mechanical strength to drug location. *Acta Biomater.* **2010**, *6*, 266-274.

[44] Talmon, Y. *Electron Beam Radiation Damage to Organic and Biological Cryospecimens*, in: *Cryotechniques in Biological Electron Microscopy*, (Eds.: R.A. Steinbrecht, K. Zierold), Springer, **1987**, pp. 64-84.

[45] Rangavittal, N.; Landa-Cánovas, A.R.; González-Calbet, J.M.; Vallet-Regí, M. Structural study and stability of hydroxyapatite and β-tricalcium phosphate: Two important bioceramics. *J. Biomed. Mater. Res.* **2000**, *51*, 660-668.

[46] Vueba, M.L.; Pina, M.E.; Batista de Carvalho, L.A. Conformational stability of ibuprofen: Assessed by DFT calculations and optical vibrational spectroscopy. *J. Pharm. Sci.* **2008**, *97*, 845-859.

[47] Williamson, M.P. Using chemical shift perturbation to characterise ligand binding. *Prog. Nucl. Magn. Reson. Spectrosc.* **2013**, *73*, 1-16.

[48] Levitt, M.; Perutz, M.F. Aromatic rings act as hydrogen bond acceptors. *J. Mol. Biol.* **1988**, *201*, 751–754.

[49] Penel, G.; Leroy, G.; Rey, C.; Sombret, B.; Huvenne, J. P.; Bres, E. Infrared and Raman microspectroscopy study of fluor-hydroxy- and hydroxyl-apatite powder. *J. Mater. Sci.-Mater. M.* **1997**, *8*, 271–276.

[50] Zhan, C.-H.; Jiang, M.-X.; Feng, Y.-L.; He, Y.-H. Syntheses, structures, network topologies and photoluminescence of four Zn(II) and Cd(II) coordination polymers based on 5-carboxyl-1-carboxymethyl-2-oxidopyridinium. *Polyhedron* **2010**, *29*, 2250–2257.

[51] Aroca, R.; Jennings, C.; Loutfy, R.O.; Hor, A.M. The structure of organic thin films: Raman polarization studies. *J. Phys. Chem.* **1986**, *90*, 5255–5257.

[52] Hédoux, A.; Guinet, Y.; Derollez, P.; Dudognon, E.; Correia, N.T. Raman spectroscopy of racemic ibuprofen: Evidence of molecular disorder in phase II. *Int. J. Pharm.* **2011**, *421*, 45-52.

[53] Hite, M.; Federici, C.; Brunelle, A.; Turner, S. Modified release ibuprofen dosage form. US9028869 B2, **2015**.

SYNOPSIS

Nanocrystalline hydroxyapatite (nanoHA) is used as a bone defect filler and to promote fracture repair or osseointegration, while ibuprofen is the most commonly used anti-inflammatory non-steroidal analgesic drug. When hydroxyapatite and ibuprofen are combined they can synergistically improve the clinical performance of these treatments. At a molecular level they both possess functional groups that can act as both hydrogen bond donors and acceptors. This study elucidates for the first time the mechanism of hydrogen bond induced ibuprofen adsorption on the surface of nanoHA crystals and shows how such interaction influences drug dissolution rates. Understanding the processes behind the active pharmaceutical ingredient attachment to the drug carrier is of paramount importance for the design of new bioactive composite materials with desirable properties.

GRAPHICAL TOC